Artificial Boundary Conditions for Nonlocal Heat Equations on Unbounded Domain

Wei Zhang[1,*], Jiang Yang[2], Jiwei Zhang[1] and Qiang Du[2]

[1] *Beijing Computational Science Research Centre, Beijing, P.R. China.*
[2] *Department of Mathematics, Columbia University, New York, NY 10027, USA.*

Abstract. This paper is concerned with numerical approximations of a nonlocal heat equation define on an infinite domain. Two classes of artificial boundary conditions (ABCs) are designed, namely, nonlocal analog Dirichlet-to-Neumann-type ABCs (global in time) and high-order Padé approximate ABCs (local in time). These ABCs reformulate the original problem into an initial-boundary-value (IBV) problem on a bounded domain. For the global ABCs, we adopt a fast evolution to enhance computational efficiency and reduce memory storage. High order fully discrete schemes, both second-order in time and space, are given to discretize two reduced problems. Extensive numerical experiments are carried out to show the accuracy and efficiency of the proposed methods.

1 Introduction

In this paper, we consider the numerical computation of 1D nonlocal heat equations on an unbounded spatial domain, given by

$$u_t(x,t) = \mathcal{L}_\delta u(x,t) + f(x,t), \quad (x,t) \in \mathbb{R} \times (0,T], \tag{1.1}$$

$$u(x,0) = g(x), \quad x \in \mathbb{R}, \tag{1.2}$$

$$u(x,t) \to 0, \quad \text{as } |x| \to \infty, \ \forall t > 0, \tag{1.3}$$

---

*Corresponding author. *Email addresses:* `wzhang@csrc.ac.cn` (W. Zhang), `jyanghkbu@gmail.com` (J. Yang), `jwzhang@csrc.ac.cn` (J. Zhang), `qd2125@columbia.edu` (Q. Du)

where the initial value $g = g(x)$ and the source $f = f(x,t)$ are the given compactly supported functions. The nonlocal operator $\mathcal{L}_\delta$ is defined as

$$\mathcal{L}_\delta u(x) = \int_{\mathbf{B}_\delta(x)} (u(x') - u(x))\gamma_\delta(x,x')dx', \qquad \forall x \in \mathbb{R}^d,$$

where $\mathbf{B}_\delta(x) = \{x' | x' \in \mathbb{R}^d : |x' - x| < \delta\}$ is a neighborhood of x with radius δ. Usually, $\gamma_\delta = \gamma_\delta(x,x') : \mathbb{R}^d \times \mathbb{R}^d \to \mathbb{R}$ is a nonnegative, radial-type kernel, namely, $\gamma_\delta(x,x') = \gamma_\delta(|x - x'|)$. Furthermore, it is compactly supported by $x' \notin \mathbf{B}_\delta(x)$ and satisfies the following second moment condition

$$0 < \int_0^\delta \tau^2 \gamma_\delta(\tau)d\tau = C_\delta < \infty. \tag{1.4}$$

Eq. (1.3) may be viewed as a nonlocal-in-space analog of the the classical heat equations [13]. Although the latter have been widely applied in many fields based on Fick's first law for local diffusive fluxes [4, 36, 37], nonlocal heat equations offer better models for anomalous diffusion behavior. Nonlocal integral operators in the form of $\mathcal{L}_\delta$ have also been used in nonlocal peridynamics models of mechanics [12, 18, 23, 39–41], thermal diffusion and electromigration [3, 7–9, 15, 17, 20]. A mathematical framework of nonlocal vector calculus and nonlocal balance laws has been developed in [14, 22]. It has been applied to study related volume-constraint problem [13, 14, 34]. Aside from mathematical analysis of PD/nonlocal models, there are also various numerical methods such as finite difference, finite element, quadrature and particle-based methods [10,16,33,49]. Recently, Tian and Du [43,44] present the deep insight for the numerical approximations to nonlocal models. Most importantly, their works address the issue of convergence in both the nonlocal setting and the local limit, and find the asymptotically compatible schemes for nonlocal models. All the above PD/nonlocal simulations focus on numerically solving problems with fixed boundary conditions on bounded domain. In fact, there are many applications in which the simulation of an infinite medium may be useful, such as wave or crack propagation, superdiffusion in a whole space.

The nonlocal heat equations/peridynamic thermal diffusion models under consideration can be formulated by the nonlocal heat transfer between material points [7,8]. In one dimensional space, the nonlocal operator becomes

$$\mathcal{L}_\delta u(x) = \int_{-\delta}^\delta [u(x+\tau) - u(x)]\gamma_\delta(\tau)d\tau. \tag{1.5}$$

With a suitably defined kernel, as $\delta \to 0$, for a smooth function $u = u(x)$, we may have $\mathcal{L}_\delta u \to a^2 d^2 u/dx^2$ for some constant $a > 0$ [13,34]. Thus, the nonlocal model (1.1)-(1.3) in the local limit tends to the classical heat equation

$$u_t(x,t) = a^2 u_{xx}(x,t) + f(x,t), \quad (x,t) \in \mathbb{R} \times (0,T], \tag{1.6}$$

$$u(x,0) = g(x), \quad x \in \mathbb{R}, \tag{1.7}$$

$$u \to 0, \quad \text{as } |x| \to \infty. \tag{1.8}$$

The artificial boundary method (ABM) is a useful approach to deal with problems on unbounded domain [26]. The main idea of ABM is firstly to introduce artificial boundaries to limit the computational domain of interest, then construct suitable artificial/absorbing boundary conditions (ABCs) on artificial boundaries, finally reformulate the problem on unbounded domain into a problem on bounded domain. Another approach to simulate an infinite medium by absorbing any impinging waves at the computational boundaries is the perfectly matched layer (PML), which was originally introduced for electromagnetic simulations [6, 11]. Recently, PML approach facilitated with an auxiliary field formulation has been applied to simulate peridynamics [45, 46].

In the last three decades, there have been numerous studies on the numerical solution of the classical heat equation in an unbounded domain via global and local ABCs, see [21, 24, 25, 47]. However, the design of ABCs for nonlocal heat equation remains open. In this paper, we consider effective ABCs for nonlocal heat equation on unbounded domain. The main challenge is that a nonlocal operator is generically associated with volume constrained boundary conditions. This motivates us to introduce a layer to surround the computational domain of interest, and design suitable boundary conditions on the artificial layer. This differs from the traditional ABCs defined on a co-dimensional one surface. Inspired by the derivation of ABCs for local heat equations in [47], we first consider a problem on exterior domain, and obtain an approximate general solution to a nonlocal differential equations in the Laplace space. Using boundary conditions at infinity and the inverse Laplace transformation, we enforce the out-going wave condition and obtain a relationship between the differential operator in nonlocal sense, which is like a one-way operator similar to the classical Dirichlet-to-Neumann (DtN)-type ABCs. These one-side nonlocal operators make the system solvable on the bounded domain.

The above obtained ABCs on artificial layers involve the time fractional Caputo derivative ${}_{0}^{C}D_{t}^{\alpha}u(t)$ of order $\alpha = \frac{1}{2}$, which can be expressed as a convolution of $u'(t)$ with the kernel $t^{-\alpha}$. When the direct method such as L^1-approximation [32, 38, 42] is used to calculate Caputo derivative, the resulting algorithm need $\mathcal{O}(N_T^2)$ overall computational cost with N_T the total number of time steps. To overcome this excessive computational cost, we use a fast evaluation of the Caputo fractional derivative with only $\mathcal{O}(N_T n_{\exp})$ operations needed ($n_{\exp}$ being the number of exponentials, see the discussions in [30] and references therein). Another contribution of this paper is to construct high-order local ABCs by Padé expansion and the introduction of suitable auxiliary variables. The local ABCs can not only enhance the efficiency but also reduce the memory storage.

The paper is organized as follows. In Section 2, we consider the constructions of ABCs, which reformulate the problem on an unbounded domain into a problem defined on a finite domain. In Section 3, discrete schemes obtained by quadrature-based finite difference approximations are given. In Section 4, numerical experiments are presented. the numerical efficiency and stability of our approach are elucidated. A conclusion is given at the end.

2   Design of artificial boundary conditions

First, we choose the computation domain as $[x_l,x_r]$ such that both the source term f and the initial value g are compactly supported in $(x_l+\delta,x_r-\delta)$. Due to the nonlocality of the operator $\mathcal{L}_\delta$, we introduce absorbing layers (that differ from PML since we need to design suitable ABCs on these layers), defined by

$$\Gamma_- := \{x|x\in[x_l-\delta,x_l]\} \quad \text{and} \quad \Gamma_+ := \{x|x\in[x_r,x_r+\delta]\}.$$

We further divide the whole domain $\mathbb{R}$ into three parts with some overlap as

$$\Omega_- := \{x|-\infty<x<x_l+\delta\}, \quad \Omega_i := \{x|x_l<x<x_r\}, \quad \Omega_+ := \{x|x_r-\delta<x<\infty\}.$$

We can put these notations in the figure below for visual illustration.
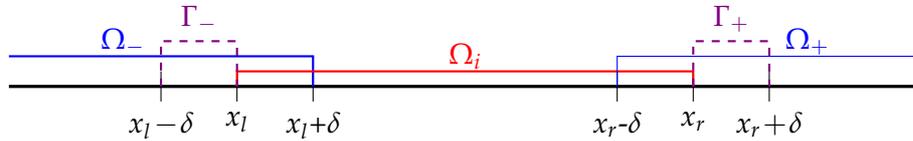
To construct effective boundary conditions, we first consider two sub-problems on the exterior domains Ω_- and Ω_+. Let us denote $\Omega_e = \Omega_-\cup\Omega_+$, then

$$u_t(x,t) = a^2\mathcal{L}_\delta u(x,t), \quad (x,t)\in\Omega_e\times(0,T], \tag{2.1}$$

$$u(x,0) = 0, \quad x\in\Omega_e, \tag{2.2}$$

$$u\to 0, \quad \text{as } |x|\to\infty. \tag{2.3}$$

Applying Laplace transform to (2.1), we arrive at

$$s\hat{u} = a^2\int_{-\delta}^{\delta}[\hat{u}(x+\tau,s)-\hat{u}(x,s)]\gamma_\delta(\tau)d\tau. \tag{2.4}$$

The Laplace transformation and its inverse transformation are given by

$$\mathfrak{L}\{f(t);s\} = \widehat{f}(s) = \int_0^{+\infty}e^{-st}f(t)dt, \quad \text{Re}(s)>0,$$

$$\mathfrak{L}^{-1}\{\widehat{g}(s);t\} = g(t) = \frac{1}{2\pi i}\int_{-i\infty}^{+i\infty}e^{st}\hat{g}(s)ds, \quad i^2 = -1.$$

Generally, it is not feasible to construct the exact solution $\hat{u}$ to Eq. (2.4) since the right-hand-side of (2.4) is an integral having a general kernel. However, we observe that Eq. (2.4) has a general solution in the form $\hat{u}(x,s) = ce^{-\lambda(s)x}$, in which both the constant c and $\lambda(s)$ are undetermined. Plugging such a solution into (2.4) yields

$$s = a^2\int_0^{\delta}(e^{-\lambda\tau}-2+e^{\lambda\tau})\gamma_\delta(\tau)d\tau, \tag{2.5}$$

where the symmetry of the kernel γ_δ is used. Although we get a nonlinear relation between s and $\lambda(s)$, it is nontrivial to write down the exact expression for Eq. (2.5). Alternatively, we turn to its approximation by applying Taylor expansion on $e^{-\lambda\tau}$ and $e^{\lambda\tau}$ up to order $\mathcal{O}((\lambda\tau)^4)$, and using the fact $\int_0^\delta \tau^2\gamma_\delta(\tau)d\tau = 1$. We then arrive at

$$
\begin{aligned}
s &= a^2\int_0^\delta (\lambda^2\tau^2+\mathcal{O}((\lambda\tau)^4))\gamma_\delta(\tau)d\tau \\
&\approx a^2\lambda^2.
\end{aligned}
\tag{2.6}
$$

Thus we approximate $\lambda(s)$ as

$$
\lambda_{1,2}(s) = \pm\sqrt[+]{s/a^2},
\tag{2.7}
$$

where $\sqrt[+]{\cdot}$ represents the square root with positive real part. Considering the boundary conditions at infinity, we have a class of estimated solutions in the frequency domain for two sub-problems as

$$
\hat{u}(x,s) = c_1 e^{\sqrt[+]{s/a^2}x}, x\in\Omega_-, \quad\text{and}\quad \hat{u}(x,s) = c_2 e^{-\sqrt[+]{s/a^2}x}, \quad x\in\Omega_+, \quad c_i\in\mathbb{R}.
\tag{2.8}
$$

To improve the order to $\mathcal{O}((\lambda\tau)^6)$ in the Taylor expansion, we have

$$
s = a^2\int_0^\delta\left(\lambda^2\tau^2+\frac{\lambda^4\tau^4}{12}+\mathcal{O}((\lambda\tau)^6)\right)\gamma_\delta(\tau)d\tau.
\tag{2.9}
$$

This leads to more complicated and delicate approximations. As the first step, we derive boundary conditions using approximated solutions in (2.8), taking into account of the nonlocality of the nonlocal diffusion operator. Hence, a one-side nonlocal operator is introduced on either the left or the right boundary layer respectively by

$$
N_R(u(x,t)) = \int_0^\delta (u(x,t)-u(x-\tau,t))\tau\gamma_\delta(\tau)d\tau, \qquad x\in\Gamma_+,
\tag{2.10}
$$

$$
N_L(u(x,t)) = \int_0^\delta (u(x+\tau,t)-u(x,t))\tau\gamma_\delta(\tau)d\tau, \qquad x\in\Gamma_-.
\tag{2.11}
$$

It can be verified that $N_L(u)$ and $N_R(u)$ tend to the left and the right derivatives of u respectively as $\delta\to 0$ [13–15, 35].

2.1 Designing global artificial boundary conditions

We firstly consider the right artificial boundary layer Γ_+. Applying Laplace transformation to the operator (2.10), we have

$$
\mathfrak{L}\{N_R(u(x,t))\} = N_R(\hat{u}(x,s)) = \int_0^\delta (\hat{u}(x,s)-\hat{u}(x-\tau,s))\tau\gamma_\delta(\tau)d\tau, \qquad x\in\Gamma_+.
\tag{2.12}
$$

As N_R is defined in $\Gamma_+ = [x_r, x_r + \delta]$ with a nonlocal horizon parameter δ, its domain of definition includes $[x_r - \delta, x_r + 2\delta] \subset \Omega_+$. Substituting the approximated solutions $\hat{u}(x,s) = ce^{\lambda_1(s)x}$ with $\lambda_1(s) = -\sqrt[+]{s/a^2}$ into (2.12) yields

$$N_R(\hat{u}(x,s)) = \hat{u}(x,s) \int_0^\delta (1 - e^{-\lambda_1 \tau}) \tau \gamma_\delta(\tau) d\tau$$

$$\approx -\sqrt[+]{s/a^2} \hat{u} - \frac{s}{2a^2} \hat{u} \int_0^\delta \tau^3 \gamma_\delta(\tau) d\tau, \tag{2.13}$$

where in the last step we replace $e^{-\lambda_1 \tau}$ with $1 - \lambda_1 \tau + \frac{1}{2}\lambda_1^2 \tau^2$. Taking Laplace inverse transformation on (2.13), we get the boundary condition on the right side

$$N_R(u(x,t)) = -\sqrt{\frac{1}{a^2}} {}_0^C D_t^{\frac{1}{2}} u(x,t) - \frac{1}{2a^2} \partial_t u(x,t) \int_0^\delta \tau^3 \gamma_\delta(\tau) d\tau, \quad x \in \Gamma_+, \tag{2.14}$$

where ${}_0^C D_t^{\frac{1}{2}}$ represents the Caputo fractional derivative of order $\frac{1}{2}$, defined by

$$ {}_0^C D_t^{\frac{1}{2}} u(x,t) = \frac{1}{\Gamma(1-\frac{1}{2})} \int_0^t \frac{u_\tau(x,\tau)}{(t-\tau)^{\frac{1}{2}}} d\tau.$$

Similarly, we have the boundary condition on the left

$$N_L(u(x,t)) = \sqrt{\frac{1}{a^2}} {}_0^C D_t^{\frac{1}{2}} u(x,t) + \frac{1}{2a^2} \partial_t u(x,t) \int_0^\delta \tau^3 \gamma_\delta(\tau) d\tau, \quad x \in \Gamma_-. \tag{2.15}$$

Combining conditions (2.14) and (2.15), the problem (1.1)-(1.3) on the unbounded domain is reduced to an IBV problem on a bounded domain

$$\begin{cases} u_t = a^2 \mathcal{L}_\delta u + f(x,t), & x \in \Omega_i, \\ u(x,0) = g(x), & x \in \Omega_i \cup \Gamma_+ \cup \Gamma_-, \\ N_R(u(x,t)) = -\sqrt{\frac{1}{a^2}} {}_0^C D_t^{\frac{1}{2}} u(x,t) - \frac{1}{2a^2} \partial_t u(x,t) \int_0^\delta \tau^3 \gamma_\delta(\tau) d\tau, & x \in \Gamma_+, \\ N_L(u(x,t)) = \sqrt{\frac{1}{a^2}} {}_0^C D_t^{\frac{1}{2}} u(x,t) + \frac{1}{2a^2} \partial_t u(x,t) \int_0^\delta \tau^3 \gamma_\delta(\tau) d\tau, & x \in \Gamma_-. \end{cases} \tag{2.16}$$

Remark 2.1. Our newly derived ABCs (2.14) and (2.15) are consistent with the classical heat equation in the case $\delta \to 0$. For example, taking the constant kernel $\gamma_\delta(\tau) = 3\delta^{-3}$, the ABCs becomes

$$N_R(u(x,t)) = -\sqrt{\frac{1}{a^2}} {}_0^C D_t^{\frac{1}{2}} u(x,t) - \frac{3\delta}{8a^2} \partial_t u(x,t), \quad x \in \Gamma_+, \tag{2.17}$$

$$N_L(u(x,t)) = \sqrt{\frac{1}{a^2}} {}_0^C D_t^{\frac{1}{2}} u(x,t) + \frac{3\delta}{8a^2} \partial_t u(x,t), \quad x \in \Gamma_-. \tag{2.18}$$

One can see that as δ approaches to 0, the ABCs (2.17) and (2.18) respectively reduce to

$$u_x(x_r,t) = -\sqrt{\frac{1}{a^2}}{}_0^C D_t^{\frac{1}{2}} u(x_r,t) \tag{2.19}$$

$$u_x(x_l,t) = \sqrt{\frac{1}{a^2}}{}_0^C D_t^{\frac{1}{2}} u(x_l,t), \tag{2.20}$$

which are the same as the exact global ABCs for the classical heat equations (1.6)-(1.8). This in fact holds for all nonnegative kernels satisfying second moment condition (1.4).

Remark 2.2. We note that the approach for designing the ABCs for nonlocal models (2.17) and (2.18) follows form the derivation of the exact global artificial boundary conditions (2.19) and (2.20). But the idea of introducing the one-side nonlocal operators to close the whole system is new. This is a crucial step to reduce the original problem on infinite domain to a bounded domain. Even when the kernels in N_R and N_L are different from the one in $\mathcal{L}_\delta$, the approach is still applicable. For simplicity, we choose the constant kernel in both N_R and N_L regardless of whichever kernel is used in $\mathcal{L}_\delta$.

2.2   Designing high-order artificial boundary conditions

Since the nonlocal boundary conditions (2.14) and (2.15) are global in time, it is natural to consider high-order approximate ABCs that are local in time in order to reduce the computation and memory cost. Similar to the technique given by Engquist and Majda [19], we use the Padé expansion to approximate the square root by

$$\sqrt{s} \approx \sqrt{z_0}\left(1 + \sum_{i=1}^{p}\frac{b_i}{a_i} - \sum_{i=1}^{p}\frac{b_i}{a_i}\frac{z_0}{z_0 - a_i(z_0 - s)}\right), \tag{2.21}$$

where $a_i = \cos^2\frac{i\pi}{2p+1}$, $b_i = \frac{2}{2p+1}\sin^2\frac{i\pi}{2p+1}$, $i = 1,\cdots,p$. Substituting the Padé approximation (2.21) into (2.13), and introducing the auxiliary variables

$$\hat{\omega}_i(x,t) = \frac{1}{z_0 - a_i(z_0 - s)}\hat{u}(x,t), \quad x \in \Gamma_+, \tag{2.22}$$

we obtain an approximated system on the right-side boundary layer

$$\begin{cases} aN_R(\hat{u}) = -\sqrt{z_0}\left[\left(1 + \sum_{i=1}^{p}\frac{b_i}{a_i}\right)\hat{u} - z_0\sum_{i=1}^{p}\frac{b_i}{a_i}\hat{\omega}_i\right] - \frac{s}{2a}\hat{u}\int_0^\delta \tau^3\gamma_\delta(\tau)d\tau, & x \in \Gamma_+, \\ (z_0 - a_iz_0 + a_is)\hat{\omega}_i = \hat{u}, & x \in \Gamma_+. \end{cases} \tag{2.23}$$

In the same vein, we introduce auxiliary variables

$$\hat{\mu}_i(x,t) = \frac{1}{z_0 - a_i(z_0 - s)}\hat{u}(x,t), \quad x \in \Gamma_-, \tag{2.24}$$

and get a corresponding approximated system on the left-side boundary layer

$$
\begin{cases}
aN_L(\hat{u}) = \sqrt{z_0}\left[\left(1+\sum_{i=1}^{p}\frac{b_i}{a_i}\right)\hat{u}-z_0\sum_{i=1}^{p}\frac{b_i}{a_i}\hat{\mu}_i\right]+\frac{s}{2a}\hat{u}\int_0^{\delta}\tau^3\gamma_{\delta}(\tau)d\tau, & x\in\Gamma_-, \\
(z_0-a_iz_0+a_is)\hat{\mu}_i = \hat{u}, & x\in\Gamma_-.
\end{cases}
\tag{2.25}
$$

Applying the inverse Laplace transform on nonlocal boundary conditions (2.23) and (2.25), we reduce the original problem (1.1)-(1.3) to an IBV problem on a bounded domain with the Padé approximation based local-in-time ABCs (abbreviated as Padé ABCs)

$$
\begin{cases}
u_t = a^2\mathcal{L}_{\delta}u+f(x,t), & x\in\Omega_i, \\
u(x,0) = g(x), & x\in\Omega_i, \\
aN_R(u) = -\sqrt{z_0}\left[\left(1+\sum_{i=1}^{p}\frac{b_i}{a_i}\right)u-z_0\sum_{i=1}^{p}\frac{b_i}{a_i}\omega_i\right]-\frac{1}{2a}u_t\int_0^{\delta}\tau^3\gamma_{\delta}(\tau)d\tau, & x\in\Gamma_+, \\
(z_0-a_iz_0)\omega_i+a_i\partial_t\omega_i = u(x,t), & i=1,2,\cdots,p, & x\in\Gamma_+, \\
aN_L(u) = \sqrt{z_0}\left[\left(1+\sum_{i=1}^{p}\frac{b_i}{a_i}\right)u-z_0\sum_{i=1}^{p}\frac{b_i}{a_i}\mu_i\right]+\frac{1}{2a}u_t\int_0^{\delta}\tau^3\gamma_{\delta}(\tau)d\tau, & x\in\Gamma_-, \\
(z_0-a_iz_0)\mu_i+a_i\partial_t\mu_i = u(x,t), & i=1,2,\cdots,p, & x\in\Gamma_-.
\end{cases}
\tag{2.26}
$$

3   Fully discrete scheme

We adopt the quadrature-based 2nd order finite difference method examined in [43] to discretize nonlocal operators $\mathcal{L}_{\delta}$, N_L and N_R on a uniform grid on $\Omega_i:=(x_l,x_r)$ with $h=\frac{x_r-x_l}{N_x+1}$ and $\Delta t=\frac{T}{N_t}$ on $[0,T]$ with $N_x,N_t\in\mathbb{Z}^+$. Denote $t_n=n\Delta t,(n=0,1,\cdots,N_t)$, $I_j=((j-1)h,jh)$ for $1\le j\le r$. Here we only consider the case when $\delta=rh$ for some integer $r>1$.

Let $x_j=x_l+jh$, where $j\in\Omega_i^h=\{1,\cdots,N_x\}$ for internal point, $j\in\Gamma_-^h=\{-r,\dots,0\}$ for left-side boundary layer and $j\in\Gamma_+^h=\{N_x+1,\cdots,N_x+r+1\}$ for the right-side. Let the piecewise linear hat basis functions be given by

$$
\phi_k^1(x) = \begin{cases}
(x-(k-1)h)/h, & x\in I_k, \\
((k+1)h-x)/h, & x\in I_{k+1}, \\
0, & \text{otherwise}.
\end{cases}
\tag{3.1}
$$

With u_j^n representing the approximation of $u(x_j,t_n)$, and noticing that $\sum_{k=0}^{r}\phi_k^1(\cdot)=1$, we can reformulate (1.5) in the following form

$$
\begin{aligned}
\mathcal{L}_{\delta}u(x) &= \int_0^{\delta}\frac{u(x+\tau)-2u(x)+u(x-\tau)}{\tau^{\alpha}}\tau^{\alpha}\gamma_{\delta}(\tau)d\tau \\
&= \sum_{k=0}^{r}\int_0^{\delta}\frac{u(x+\tau)-2u(x)+u(x-\tau)}{\tau^{\alpha}}\tau^{\alpha}\phi_k^1(\tau)\gamma_{\delta}(\tau)d\tau.
\end{aligned}
\tag{3.2}
$$

Then we take the quadrature collocation scheme given in [43] to discretize the nonlocal diffusion operator $\mathcal{L}_\delta^h$ as

$$\mathcal{L}_\delta^h(u_j) = \sum_{k=1}^r \frac{u_{j+k} - 2u_j + u_{j-k}}{(kh)^\alpha} \int_0^\delta \tau^\alpha \phi_k^1(\tau)\gamma_\delta(\tau)d\tau. \tag{3.3}$$

By setting $\alpha = 1$, we have the internal nonlocal stiffness matrix $A_\delta = (a_{ij})$ based on the quadrature collocation method that is designed to be second order accurate in space. Denote $k = |j-i|$, then

$$a_{ij} = \begin{cases} -2\left(\displaystyle\sum_{k=1}^{r-1} \frac{1}{kh} \int_{I_k \cup I_{k+1}} \phi_k^1(\tau)\tau\gamma_\delta(\tau)d\tau + \frac{1}{rh} \int_{I_r} \phi_r^1(\tau)\tau\gamma_\delta(\tau)d\tau\right), & k=0, \\[4mm] \dfrac{1}{kh} \displaystyle\int_{I_k \cup I_{k+1}} \phi_k^1(\tau)\tau\gamma_\delta(\tau)d\tau, & 1 \le k \le r-1, \\[4mm] \dfrac{1}{rh} \displaystyle\int_{I_r} \phi_r^1(\tau)\tau\gamma_\delta(\tau)d\tau, & k=r, \\[4mm] 0, & \text{otherwise.} \end{cases} \tag{3.4}$$

On the boundary layers, or boundary interaction domains, we follow the same idea and use quadrature-based finite difference discretization, with $k = i-j$ for the boundary on the right-side and $k = j-i$ on the left-side,

$$\begin{aligned} N_R^h(u_i) &= \sum_{k=1}^r \frac{u_i - u_{i-k}}{(kh)^\alpha} \int_0^\delta \phi_k^1(\tau)\tau^{1+\alpha}\gamma_\delta(\tau)d\tau \\ &= \sum_{k=1}^{r-1} \frac{u_i - u_{i-k}}{(kh)^\alpha} \int_{I_k \cup I_{k+1}} \phi_k^1(\tau)\tau^{1+\alpha}\gamma_\delta(\tau)d\tau + \frac{(u_i - u_{i-r})}{(rh)^\alpha} \int_{I_r} \phi_r^1(\tau)\tau^{1+\alpha}\gamma_\delta(\tau)d\tau, \end{aligned}$$

where u_i is the numerical approximation of $u(x_i)$. We take $\alpha = 0$ in the numerical examples for these boundary approximations.

In time, we take the second-order Crank-Nicolson scheme to match with the second-order spatial accuracy.

3.1 Discrete scheme of global artificial boundary conditions

In this section, we present the fast evaluation of the fractional Caputo derivative to numerically solve the problem (2.16). The main procedure is to split the convolution integral of the fractional Caputo derivative (2.1) into the sum of a local part and a historical part, given by

$$\begin{aligned} {}_0^C D_t^{\frac{1}{2}} u^n &= \frac{1}{\Gamma(1-\frac{1}{2})} \int_{t_{n-1}}^{t_n} \frac{u'(s)ds}{(t_n-s)^{\frac{1}{2}}} + \frac{1}{\Gamma(1-\frac{1}{2})} \int_0^{t_{n-1}} \frac{u'(s)ds}{(t_n-s)^{\frac{1}{2}}} \\ &:= C_l(t_n) + C_h(t_n). \end{aligned} \tag{3.5}$$

For the local part $C_l(t_n)$, we apply the standard L^1-approximation given by

$$C_l(t_n) \approx \frac{u(t_n) - u(t_{n-1})}{\Delta t \Gamma(1 - \frac{1}{2})} \int_{t_{n-1}}^{t_n} \frac{1}{(t_n - s)^{\frac{1}{2}}} ds = \frac{u(t_n) - u(t_{n-1})}{\Delta t^{\frac{1}{2}} \Gamma(\frac{3}{2})}. \tag{3.6}$$

For the historical part, we apply the integration by part to eliminate $u'(s)$ and get

$$C_h(t_n) = \frac{1}{\Gamma(\frac{3}{2})} \left[\frac{u(t_{n-1})}{\Delta t^{\frac{1}{2}}} - \frac{u(t_0)}{t_n^{\frac{1}{2}}} - \frac{1}{2} \int_0^{t_{n-1}} \frac{u(s) ds}{(t_n - s)^{\frac{3}{2}}} \right]. \tag{3.7}$$

The sum-of-exponentials approximations have been applied to speed up the evaluation of the convolution integrals in many applications, for instances, to accelerate the evaluation of the exact ABCs for the wave, Schrödinger, heat equations and fractional integrals in [1,2,5,27–31,48]. In our work, we use the approach proposed in [30] to approximate $t^{-\frac{3}{2}}$ via a sum-of-exponentials approximation for the given interval $[\Delta t, T]$ and the absolute error ε. That is to say, there exist positive real numbers s_i and w_i $(i = 1, \cdots, N_{\exp})$ such that

$$\left| \frac{1}{t^{1+\frac{1}{2}}} - \sum_{i=1}^{N_{\exp}} \omega_i e^{-s_i t} \right| \leq \varepsilon, \quad t \in [\Delta t, T], \tag{3.8}$$

where the number of exponentials $N_{\exp}$ needed is of the order (see Table 1 for example)

$$\mathcal{O} \left(\log \frac{1}{\varepsilon} \left(\log\log \frac{1}{\varepsilon} + \log \frac{T}{\Delta t} \right) + \log \frac{1}{\Delta t} \left(\log\log \frac{1}{\varepsilon} + \log \frac{1}{\Delta t} \right) \right).$$

Table 1: Number of exponentials $N_{\exp}$ needed to approximate $t^{-\frac{3}{2}}$ with fixed $\Delta t = 10^{-3}$.

$\varepsilon \backslash \frac{T}{\Delta t}$	10^3	10^4	10^5	10^6
10^{-3}	28	30	35	38
10^{-6}	42	47	47	51
10^{-9}	49	55	64	72

Replacing the convolution kernel $t^{-\frac{3}{2}}$ in (3.7) by its sum-of-exponentials approximation in (3.8), we have the historical part defined as follows:

$$C_h(t_n) \approx \frac{1}{\Gamma(1 - \frac{1}{2})} \left[\frac{u(t_{n-1})}{\Delta t^{\frac{1}{2}}} - \frac{u(t_0)}{t_n^{\frac{1}{2}}} - \frac{1}{2} \sum_{i=1}^{N_{\exp}} U_{\text{hist,i}}(t_n) \right], \tag{3.9}$$

where $U_{\text{hist,i}}(t_n)$ is given by

$$U_{\text{hist,i}}(t_n) = \omega_i \int_0^{t_{n-1}} e^{-(t_n - \tau) s_i} u(\tau) d\tau. \tag{3.10}$$

We note that $U_{\text{hist,i}}(t_n)$ satisfies the simple recurrence relation:

$$U_{\text{hist,i}}(t_n) = e^{-s_i \Delta t} U_{\text{hist,i}}(t_{n-1}) + \int_{t_{n-2}}^{t_{n-1}} e^{-s_i(t_n-\tau)} u(\tau) d\tau, \quad \text{for } n=1,2,\cdots,N_T \qquad (3.11)$$

with $U_{\text{hist,i}}(t_0)=0$ for $i=1,\cdots,N_{\exp}$. The integral on the right hand side of (3.11) is calculated by interpolating u via a linear function, and the resulting approximation is given by

$$\int_{t_{n-2}}^{t_{n-1}} e^{-s_i(t_n-\tau)} u(\tau) d\tau \approx \frac{e^{-s_i \Delta t}}{s_i^2 \Delta t} \left[(e^{-s_i \Delta t} - 1 + s_i \Delta t) u^{n-1} + (1 - e^{-s_i \Delta t} - e^{-s_i \Delta t} s_i \Delta t) u^{n-2} \right].$$

We now denote the fast evaluation of the Caputo derivative by

$$_0^{FC}\mathbb{D}_t^{\frac{1}{2}} u^n = \frac{u(t_n) - u(t_{n-1})}{\Delta t^{\frac{1}{2}} \Gamma(\frac{3}{2})} + \frac{1}{\Gamma(1-\frac{1}{2})} \left[\frac{u(t_{n-1})}{\Delta t^{\frac{1}{2}}} - \frac{u(t_0)}{t_n^{\frac{1}{2}}} - \frac{1}{2} \sum_{i=1}^{N_{\exp}} U_{\text{hist,i}}(t_n) \right]. \qquad (3.12)$$

One can observe that the above fast evaluation for the fractional Caputo derivative only needs $\mathcal{O}(1)$ work to compute $U_{\text{hist,i}}(t_n)$ at each time step since $U_{\text{hist,i}}(t_{n-1})$ is known at that point. Thus, the total work is reduced from $\mathcal{O}(N_T^2)$ for direct method to $\mathcal{O}(N_T N_{\exp})$, and the total memory requirement is reduced from $\mathcal{O}(N_T)$ for direct method to $\mathcal{O}(N_{\exp})$.

Remark 3.1. The approximation $_0^{FC}\mathbb{D}_t^{\frac{1}{2}} u^n$ in (3.12) has an error bound as follows. Suppose that $u(t) \in C^2[0,t_n]$ and let $^F R^n u := _0^C D_t^{\frac{1}{2}} u(t)\big|_{t=t_n} - _0^{FC}\mathbb{D}_t^{\frac{1}{2}} u^n$, then

$$|^F R^n u| \le C \Delta t^{\frac{3}{2}} \max_{0 \le t \le t_n} |u''(t)| + t_{n-1} \varepsilon \max_{0 \le t \le t_{n-1}} |u(t)|. \qquad (3.13)$$

Combining with the fast evaluation of Caputo fractional derivative, we can discrete the problem (2.16) by

$$\begin{cases}
D_t^+ u_j^n = a^2 \mathcal{L}_\delta^h u_j^{n+\frac{1}{2}} + f_j^{n+1/2}, & j \in \Omega_i^h, \\
u_j^0 = g_j^0, & j \in \Omega_i^h, \\
N_R^h(u_j^{n+\frac{1}{2}}) = -\sqrt{\frac{1}{a^2}} _0^{FC} D_t^{\frac{1}{2}} u_j^n - \frac{1}{2a^2} D_t^+ u_j^n \int_0^\delta \tau^3 \gamma_\delta(\tau) d\tau, & j \in \Gamma_+^h, \\
N_L^h(u_j^{n+\frac{1}{2}}) = \sqrt{\frac{1}{a^2}} _0^{FC} D_t^{\frac{1}{2}} u_j^n + \frac{1}{2a^2} D_t^+ u_j^n \int_0^\delta \tau^3 \gamma_\delta(\tau) d\tau, & j \in \Gamma_-^h,
\end{cases} \qquad (3.14)$$

where notations like

$$v_j^{n+\frac{1}{2}} = \frac{v_j^{n+1} + v_j^n}{2}, \quad D_t^+ v_j^n = \frac{v_j^{n+1} - v_j^n}{\Delta t}$$

are used.

3.2 Discrete scheme of Padé ABCs

Adopting the same finite difference method and notation, we readily have the discrete form of the reduced problem with the Padé based local-in-time ABCs (2.26) as follows:

$$
\begin{cases}
D_t^+ u_j^n = a^2 \mathcal{L}_\delta^h u_j^{n+\frac{1}{2}} + f_j^{n+\frac{1}{2}}, & j \in \Omega_i^h, \\[2mm]
u_j^0 = g_j^0, & j \in \Omega_i^h, \\[2mm]
a N_R^h(u_j^{n+\frac{1}{2}}) = -\sqrt{z_0}\left[(1+\sum_{i=1}^p \frac{b_i}{a_i})u_j^{n+\frac{1}{2}} - z_0 \sum_{i=1}^p \frac{b_i}{a_i}\omega_{i,j}^{n+\frac{1}{2}}\right] - \frac{D_t^+ u_j^n}{2a}\int_0^\delta \tau^3 \gamma_\delta(\tau)d\tau, & j \in \Gamma_+^h, \\[2mm]
(z_0 - a_i z_0)\omega_{i,j}^{n+\frac{1}{2}} + a_i D_t^+ \omega_{i,j}^{n+\frac{1}{2}} = u_j^{n+\frac{1}{2}}, \qquad i=1,2,\cdots,p, & j \in \Gamma_+^h, \\[2mm]
a N_L^h(u_j^{n+\frac{1}{2}}) = \sqrt{z_0}\left[(1+\sum_{i=1}^p \frac{b_i}{a_i})u_j^{n+\frac{1}{2}} - z_0 \sum_{i=1}^p \frac{b_i}{a_i}\mu_{i,j}^{n+\frac{1}{2}}\right] + \frac{D_t^+ u_j^n}{2a}\int_0^\delta \tau^3 \gamma_\delta(\tau)d\tau, & j \in \Gamma_-^h, \\[2mm]
(z_0 - a_i z_0)\mu_{i,j}^{n+\frac{1}{2}} + a_i D_t^+ \mu_{i,j}^{n+\frac{1}{2}} = u_j^{n+\frac{1}{2}}, \qquad i=1,2,\cdots,p, & j \in \Gamma_-^h.
\end{cases}
$$

4 Numerical results

We now give numerical examples to demonstrate the effectiveness of our ABCs, especially for high-order Padé ABCs. We check various aspects such as the dependence of the parameters z_0 and p for the Padé expansion and the dependence on the length of the computational interval. Furthermore, we investigate the asymptotic behavior of nonlocal numerical solutions as $\delta \to 0$. In the two numerical examples including high energy source and high frequency initial values, we show that our designed ABCs can absorb energy effectively. To calculate the convergence rate in space and time, we define the relative error by

$$
L_{2,ReErr}(h,\Delta t) = \frac{\|e^n\|_2}{\|u_{\delta,\text{ex}}\|_2} = \sqrt{\frac{\sum_{j=1}^{N_x}|e_j^n|^2}{\sum_{j=1}^{N_x} u_{\delta,\text{ex}}^2}}, \tag{4.1}
$$

where $e_j^n = u_{\delta,\text{ex}}(x_j,t_n) - u_{\delta,j}^n$ denotes the error on the grid point, $u_{\delta,\text{ex}}(x_j,t_n)$ denotes the exact solution of the problem (1.1)-(1.3), and $u_{\delta,j}^n$ denotes the numerical solution of the reduced problem.

4.1 Padé ABCs and global ABCs

In this part, we illustrate the effectiveness of global ABCs and Padé ABCs. In particular, we test the parameter dependence for the latter one, on P and z_0 in Padé approximation

and the length of computation domain. In this subsection, we consider a nonlocal problem in the semi-infinite interval $[-\delta,\infty)$ by imposing Dirichlet boundary conditions on left side. We construct the following exact solutions on $[-\delta,\infty)\times(0,T]$

$$u_{\delta,ex}(x,t)=e^{t-cx}, \quad (x,t)\in[-\delta,\infty)\times[0,T],$$

by setting the source term and initial value respectively as

$$f(x,t)=0, \qquad u(x,0)=e^{-cx}, \tag{4.2}$$

and the diffusion coefficient

$$a^2(\delta)=1/\left(\int_0^\delta (e^{-c\tau}-2+e^{c\tau})\gamma_\delta(\tau)d\tau\right), \tag{4.3}$$

and imposing the exact Dirichlet boundary conditions on $[-\delta,0]$ as

$$u(x,t)=e^{t-cx}, \quad x\in[-\delta,0]. \tag{4.4}$$

Hence, in the following two examples, we only need to use ABCs for the right side.

Example 4.1. We consider the problem (1.1)-(1.3) in the setting given by (4.2)-(4.4). The approximate Padé ABCs are used to solve the nonlocal equation.

First of all, we test the spatial convergence of the reduced problem with Padè ABCs (2.26). We set $x_l=1$ and $x_r=6$ such that the initial value at the artificial boundary $u(x_r,0)$ is very close to 0. We simulate the problem till the final time $T=11$ to test the effectiveness of ABCs. With a time step $\Delta t=2.75\times10^{-4}$, Figs. 1 and 2 show the effect of two Padé parameters z_0 and p respectively on the spacial convergence of the numerical scheme when taking $\Delta x=\{\frac{1}{16},\frac{1}{32},\frac{1}{64},\frac{1}{128}\}$. We compare the numerical solution $u_{\delta,j}^n$ against exact solution $u_{\delta,ex}$ on $[1,6]$ at $T=11$ and plot the relative error under $\delta=\{1,0.5,0.125,0.0625\}$. In Fig. 1, we fix $P=40$ and vary z_0. In Fig. 2 we fix $z_0=1$, change P. We observe that all spatial convergence rates are almost parallel to the second-order baseline in each subplot; the Padé ABCs are not sensitive to the choices of parameters z_0 and P involved in the Padè approximation, and the accuracy gets improved as δ is reduced. In Fig. 3, we take the same mesh size as before, fix $z_0=1$ and $P=20$, but expand the computational range gradually. Similar to last two simulations, the accuracy grows as δ gets smaller. Generally, the accuracy should increase with extended computational range. In this case, however, the change is too small to be visible. In Fig. 4, the numerical solution is shown to match with the exact solution very well. It also illustrates that the reflection is negligible at the artificial boundary. From the figures above, one can observe that long time calculations with Padè ABCs are stable.

Next we demonstrate the effectiveness of global ABCs (2.16) implemented with the fast evaluation method.
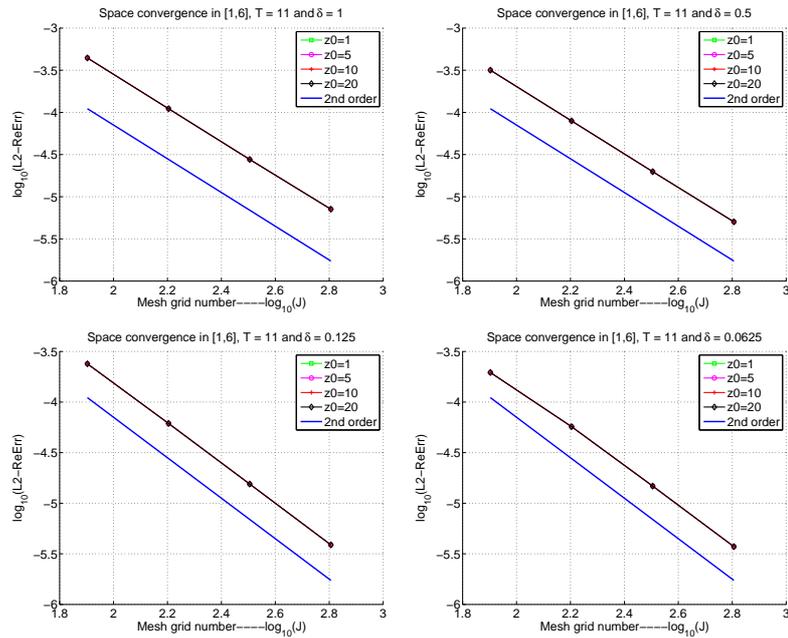
Figure 1: (Example 4.1)L^2- relative error of $u_{\delta,j}^n$ compared with nonlocal exact solutions $u_{\delta,ex}$ with different $\delta = \{1, 0.5, 0.125, 0.0625\}$ in $[1,6]$ at $T = 11$ with parameters $z_0 = \{1, 5, 10, 20\}$.
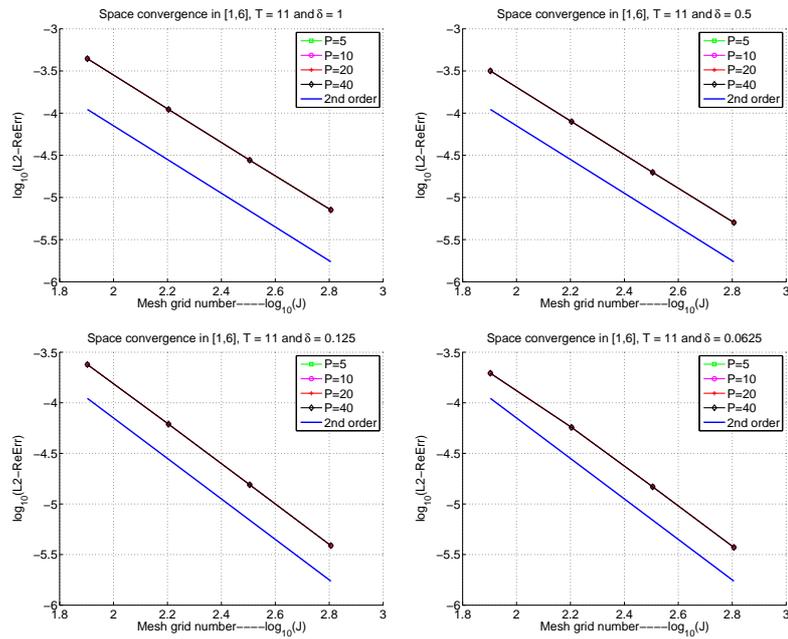
Figure 2: (Example 4.1) L^2- relative error of $u_{\delta,j}^n$ compared with nonlocal exact solutions $u_{\delta,ex}$ in $[1,6]$ at $T = 11$ with different $\delta = \{1, 0.5, 0.125, 0.0625\}$ and $P = \{5, 10, 20, 40\}$.
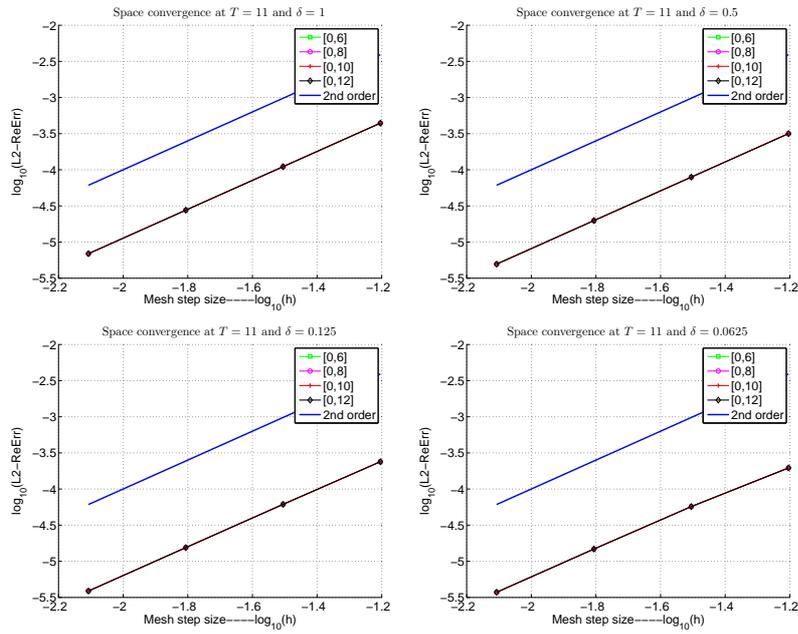
Figure 3: (Example 4.1) L^2- relative error of $u_{\delta,j}^n$ compared with nonlocal exact solutions $u_{\delta,ex}$ at $T=11$ with different computation range, and $\delta=\{1,0.5,0.125,0.0625\}$, $z_0=1,P=20$.
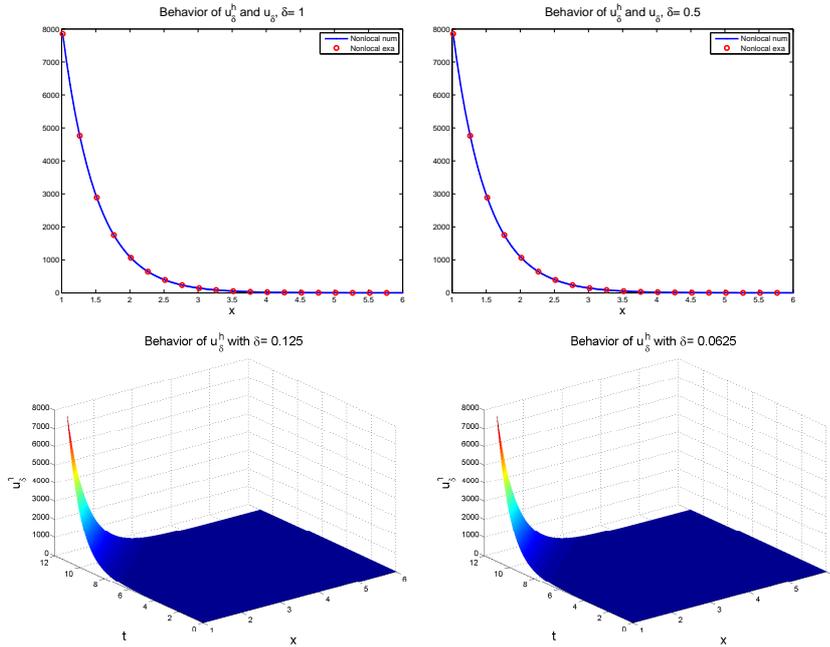
Figure 4: (Example 4.1) $u_{\delta,j}^n$ compared with nonlocal exact solutions $u_{\delta,ex}$ in $[1,6]$ at $T=11$ $\delta=\{1,0.5,0.125,0.0625\}$, and $z_0=1,P=20$.

Example 4.2. We consider the same setting as in Example 4.1, except for adopting global ABCs and fast evaluation method. The reduced problem has the form (2.16).

In this example, we take $\Delta t = 2.5 \times 10^{-6}$ and vary δ among $\{1, 0.5, 0.25, 0.125\}$ and $T = 2$. As seen in Fig. 5, the global ABCs work well and the spacial convergence of the scheme meets our expectation. The accuracy also increases as δ gets smaller. In comparison with global ABCs without fast evaluation method, this scheme works much more efficiently. In comparison with the Padé ABCs, global ones are more accurate, at the cost of more computation and memory to achieve similar accuracy. In practice, one may prefer truncated artificial boundary conditions to replace global ones without fast evaluation, this allows faster computation without significant loss in accuracy.
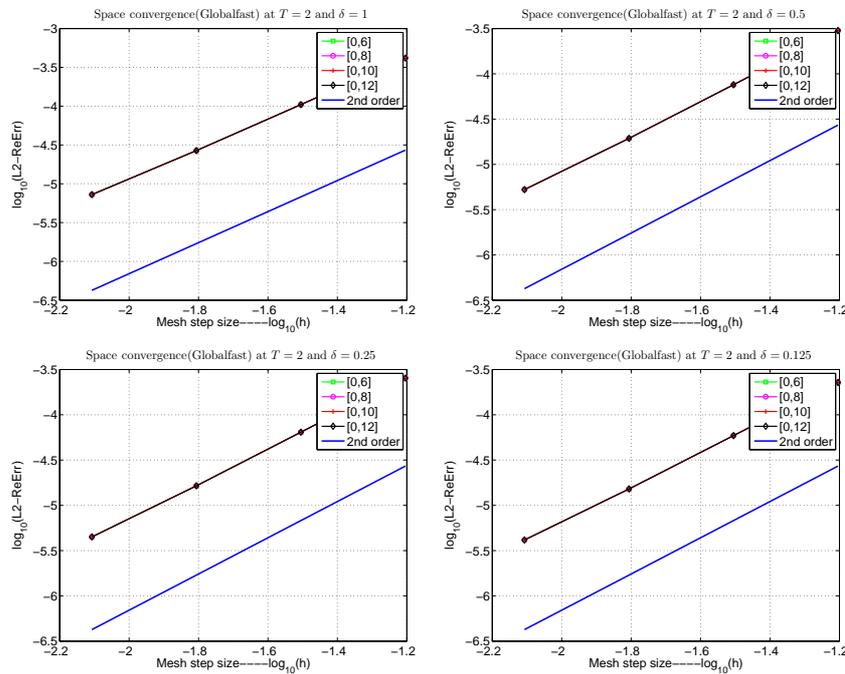
Figure 5: (Example 4.2) L^2- relative error of $u_{\delta,j}^n$ compared with nonlocal exact solutions $u_{\delta,ex}$ at $T = 2$ with different computation range, $\delta = \{1, 0.5, 0.25, 0.125\}$.

4.2   Asymptotically compatible Padé approximating ABCs

In this part, we investigate the limiting process of the nonlocal model to the classical heat equation as $\delta \rightarrow 0$, i.e. the asymptotic compatibility as first proposed and studied in [43, 44]. Here we only adopt the Padé ABCs to solve nonlocal models.

Example 4.3. First, we let the local heat equations (1.6)-(1.8) have the following Gaussian-type exact solution

$$u_{0,ex}(x,t) = \frac{1}{\sqrt{4a^2\pi(t+t_0)}}\exp\left(-\frac{x^2}{4a^2(t+t_0)}\right),$$

by choosing source term $f \equiv 0$ and imposing the local heat models with the exact initial value as

$$u_{0,ex}(x,0) = \frac{1}{\sqrt{4a^2\pi t_0}}\exp\left(-\frac{x^2}{4a^2 t_0}\right),$$

with $t_0 = 0.1$, $a = 1$. For the nonlocal problem, we take the same source term and initial data as the local one, and $a(\delta)$ is always chosen as 1. We fix the computational domain as $[-3,3]$, the final computational time $T = 6$, and $\Delta t = 1.5 \times 10^{-4}$.

We let $z_0 = 1$, $P = 20$ and decrease δ from 1 to 0.0625. Fig. 6 and Fig. 7 show the convergence of u_δ to the solution u_0 of classical local model as $\delta \to 0$. To save space, we do not plot of solution over time here. We also observe that our ABCs perform well for this nonlocal problem since no reflection is captured during simulation. Moreover, the nonlocal solutions converge to the exact local solution as δ decreases. This again confirms the asymptotic compatibility of the Padé ABCs.
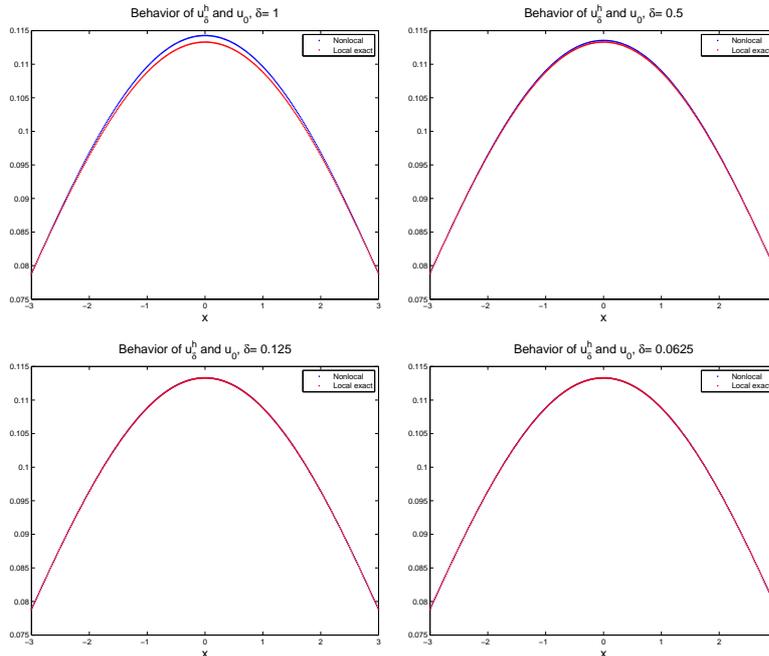
Figure 6: (Example 4.3) $u_{\delta,j}^n$ compared with local exact solution.
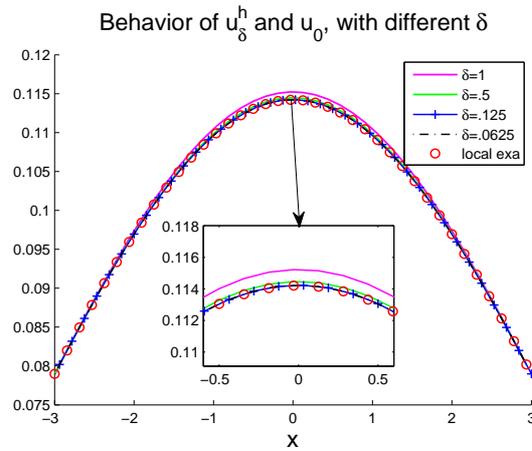
Figure 7: (Example 4.3) $u_{\delta,j}^n$ compared with local exact solution.

4.3 High energy source and highly oscillatory initial data

Using Padé ABCs, we now test two nonlocal problems with no exact solutions known a priori. One of these problems has high energy source constantly around the origin with zero initial data and the other one has high oscillating initial data with zero source term. The effectiveness of our method and numerical convergence of the difference scheme are observed. Moreover, to make a comparison, we compute the local heat problem (1.6)-(1.8) based on local Padé ABCs with the same source function and initial data. We again observe the asymptotic compatibility in the sense that $u_\delta^h \to u_0^h$ as $\delta \to 0$.

Example 4.4. For problem (1.1)-(1.3), we choose the source term $f = e^{-x^2}(x^2-9)^2\chi_{[-3,3]}$ and initial data $u(x,0) \equiv 0$, both compactly supported in $[-3,3]$. For Padé ABCs, we choose $P=20$, $z_0=1$, and set the computational domain as $[-5,5]$ and computational time $T=6$.

We first test the spatial convergence rate of out numerical scheme by fixing $\Delta t = 1.5 \times 10^{-4}$ and taking $\delta = \{0.125, 0.5, 1\}$, respectively. In Table 2, the spatial convergence order is seen to be approximately 2. When δ is large, the spatial convergence orders do not seem to be as good as those for smaller δ due to the large ratio of $\frac{\delta}{\Delta x}$. Then, we test the temporal

Table 2: (Example 4.4) Spatial convergence order at $T=6$.

	$\Delta x = \frac{1}{8}$	$\Delta x = \frac{1}{16}$	$\Delta x = \frac{1}{32}$	$\Delta x = \frac{1}{64}$	$\Delta x = \frac{1}{128}$
$\delta = 1$	-	-	1.9182	1.7447	1.4339
$\delta = 0.5$	-	-	1.9812	1.9691	1.8968
$\delta = 0.125$	-	-	1.9493	1.9869	1.9988

Table 3: (Example 4.4) Temporal convergence order at $T=6$.

	$\Delta t=\frac{1}{4}$	$\Delta t=\frac{1}{8}$	$\Delta t=\frac{1}{16}$	$\Delta t=\frac{1}{32}$	$\Delta t=\frac{1}{64}$
$\delta=1$	-	-	2.0692	2.0074	2.0007
$\delta=0.5$	-	-	2.0896	2.0102	2.0017
$\delta=0.0625$	-	-	2.1015	2.0117	2.0023

convergence order by fixing $\Delta x=\frac{1}{1024}$. As seen in Table 3, the temporal convergence of the numerical scheme is basically of second order. All these data substantiate the high order accuracy of our numerical scheme.

The snapshots of numerical nonlocal solutions and numerical local solution at $T=0.1$ and $T=6$ are shown in Fig. 8. We note that, even with zero initial value, the source term provides energy continually around the origin. Thus, the solutions increases in magnitude quite fast. The solution values at both artificial boundary domains are very large, approximately 20 at $T=6$. There is no visible reflection even for the very large energy diffusion. This indicates that the Padé approximating boundaries are indeed very effective in absorbing energy.
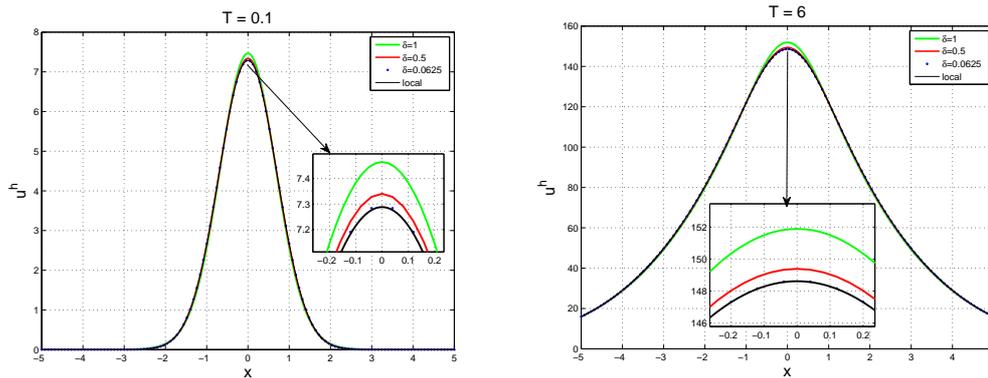
Figure 8: (Example 4.4) Nonlocal numerical solutions $u_{\delta,j}^n$ w.r.t different δ and local numerical solution $u_{0,j}^n$.

Furthermore, we look into the performance of our Padé ABCs on an example exhibiting oscillations. To this end, we design the following example.

Example 4.5. We choose the source term $f=0$, the following high frequency initial data

$$u(x,0)=\left(1+\cos(\frac{11}{3}\pi x)\right)e^{-\frac{x^2}{9}}\chi_{[-3,3]},$$

compactly supported on $(-3,3)$, and the nonlocal diffusion coefficient $a^2=0.1$. We fix the computational domain as $[-4,4]$, time step $\Delta t=0.001$ and grid width $\Delta x=2^{-8}$.

We first test numerical accuracy of our Padé ABCs. Although we do not have the exact solution, we manage to obtain a reference solution using spectral methods as follows. We choose a large enough domain $[x_a, x_b]$ such that the energy does not diffuse to the boundary of the domain. Then we can solve the problem on the large domain with periodic boundary conditions. Assume that the numerical solution has the following form

$$u_N(x,t) = \sum_{|n| \leq N} a_n(t) e^{in\frac{2\pi x}{L_x}},$$

where $L_x = x_b - x_a$. Then the Fourier coefficients $a_n(t)$s satisfy following ordinary differential equations (ODEs) respectively

$$\frac{d}{dt} a_n(t) = a^2 \lambda_\delta(n) a_n(t),$$

where $\lambda_\delta(n)$ is the nth nonlocal eigenvalue of the nonlocal diffusion operator with constant kernel, given by

$$\lambda_\delta(n) = \frac{6}{\delta^2} \left(\frac{\sin(\frac{2\pi}{L_x} n\delta)}{\frac{2\pi}{L_x} n\delta} - 1 \right).$$

We see that those ODEs can be solved exactly. So the only errors come from the spectral methods in spatial discretization. Thus we need to make sure the computational domain is large enough to guarantee the accuracy of the reference solution.

For the solutions computed by Padé ABCs, the time step $\Delta t = 0.001$ and grid size width $\Delta x = 2^{-8}$ are both fine enough to eliminate the errors contributed from discretization in spatial and time space. Hence, the dominated error is contributed from the Padé ABCs. The pointwise errors at different time are shown in Fig. 9. Except for $T = 0.1$, we see that the errors around the boundary are always larger than those inside. It is also observed that the errors become smaller as the horizon parameter decreases. This is expected as we can solve Eq. (2.5) more accurately for smaller δ. Overall, the Padé ABCs offer us one effective way to get solutions with acceptable accuracy even for large $\delta = 1$.

Moreover, we plot numerical simulations of nonlocal models with different δ against local numerical solutions u_0^h at different time in Fig. 10. Here we also compute the local solution by Padé ABCs as given in [47] with exactly the same set-up and computation parameters as for the nonlocal problem. We can see clearly the convergent trend from u_δ^h to u_0^h as δ goes 0. Before $T = 10$, the nonlocal solutions for $\delta = 1$ still exhibit some oscillations that disappear eventually, such as at $T = 10$. This provides a confirmation that the nonlocal equation with a larger horizon parameter models a slower diffusion process.

5   Conclusion

The constructions of ABCs for the nonlocal heat equation are presented in this work. There are two classes of ABCs, namely, the nonlocal analog DtN-type ABCs (global in
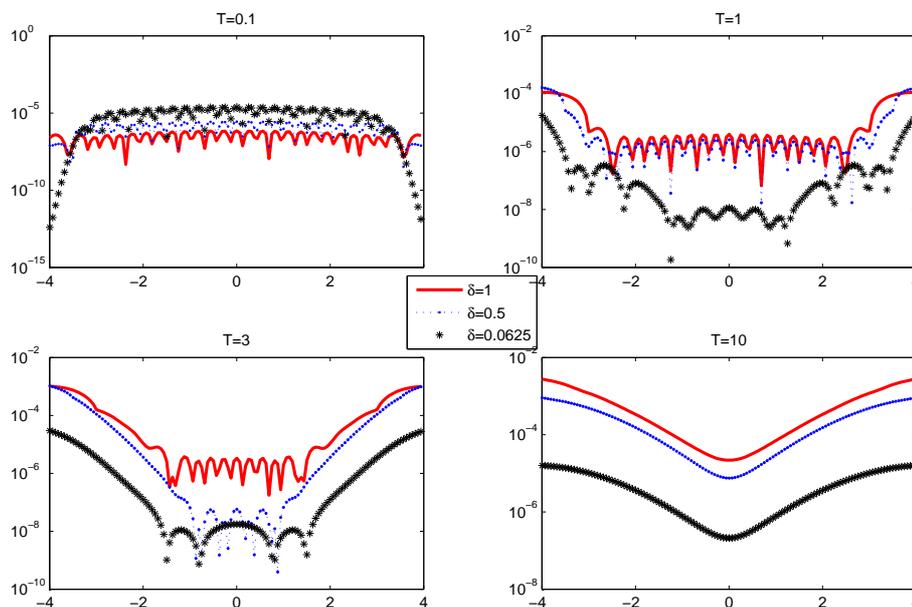
Figure 9: (Example 4.5) Pointwise errors for nonlocal solutions with Padé ABCs.
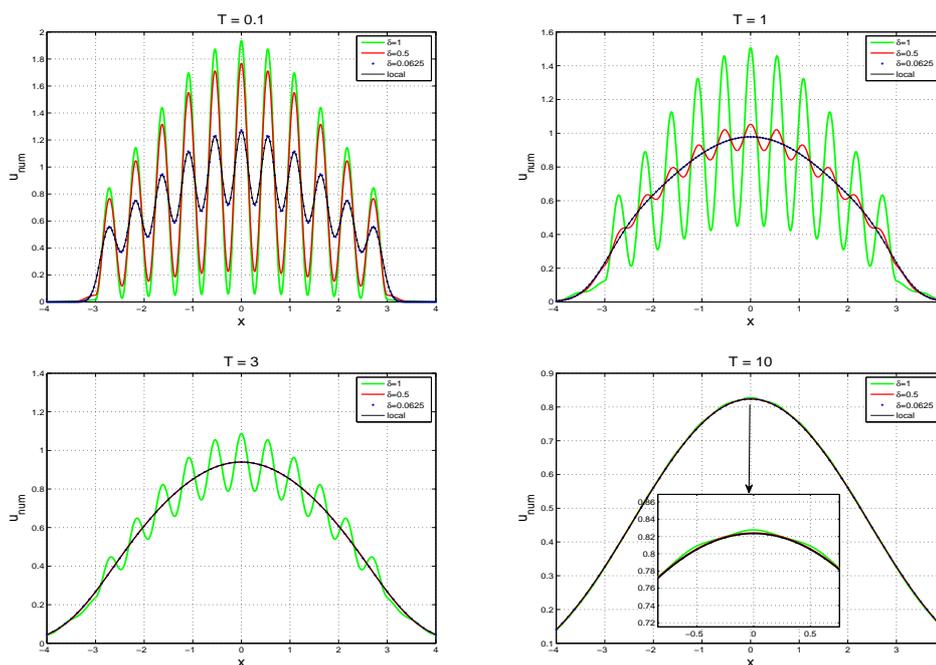
Figure 10: (Example 4.5) Numerical comparisons among nonlocal solutions $u_{\delta,j}^n$ with different δ and local solution $u_{0,j}^n$ in $[-4,4]$.

time) and high-order Padé ABCs (local in time). The former ones are nonlocal operators with the history information, and are expensive to be calculated using a direct method. The high-order Padé ABCs are a system of ODEs, which are composed of the first-order temporal derivative of some auxiliary variables. Numerical examples are given to show the effectiveness of our method and to demonstrate the robustness of our ABCs. Generally, the global ABCs are stable but expensive to implement. In this paper, we also apply the fast evaluation scheme of the Caputo fractional derivative to numerically solve the DtN-type ABCs. The resulting algorithm for solving the fractional Caputo derivative is both efficient and stable.

The current study is focused on constructing ABCs of a simple one-dimensional linear nonlocal diffusion model for the sake of offering insight without being impeded by tedious calculations. In our analysis here, we need to solve the nonlocal ODE (2.4) to obtain its eigenfunctions in the Laplace space first, then we distinguish the left-going wave and right-going wave to achieve the one-way (DtN or NtD) operator. Since it is no simple matter to get the exact expression of the solution λ in terms of s in the nonlocal ODE (2.5), we assume that the horizon parameter δ, measuring the range of nonlocal interactions, is small enough to produce the approximated eigenfunctions using the asymptotic method. For large δ, the Taylor-expansion technique may not be accurate enough to approximate (2.5). Thus, this work does not solve the nonlocality issue completely. However, the idea of introducing the one-side nonlocal operator to close the system should work in a general setting. Numerical examples demonstrate that our method works well even when the horizon parameter δ is on the same order of other parameters. In the future, further study will be carried out to address the fully nonlocal case and to consider effective algorithms in multi-dimensions. We may also to extend the study to more general nonlocal models such as nonlocal wave equations and also nonlocal continuum equations of motion in elastic solids [45, 46].

Acknowledgments

References

[1] B. Alpert, L. Greengard, and T. Hagstrom, *Rapid evaluation of nonreflecting boundary kernels for time-domain wave propagation*, SIAM J. Numer. Anal., 37 (2000), 1138-1164.

[2] B. Alpert, L. Greengard and T. Hagstrom, *Nonreflecting Boundary Conditions for the Time-Dependent Wave Equation*, Comput. Phy., 180 (2002), 270-296.

[3] F. Andreu, J.M. Mazón, J.D. Rossi, and J. Toledo, *Local and nonlocal weighted $p-$Laplacian evolution equations with Neumann boundary conditions*, Publ. Mat., 55 (2011), 27-66.

[4] O. Bakunin, *Turbulence and Diffusion: Scaling Versus Equations*, Springer-Verlag, New York, 2008.

[5] G. Beylkin and L. Monzón, *Approximation by exponential sums revisited*, Appl. Comput. Harmon. Anal., 28 (2010), 131-149.

[6] J.-P. Berenger, *A perfectly matched layer for the absorption of electromagnetic waves*, J. Comput. Phys., 114:2 (1994), 185-200.

[7] F. Bobaru and M. Duangpanya, *The peridynamic formulation for transient heat conduction*, Int. J. Heat Mass Transfer, 53 (2010), 4047-4059.

[8] F. Bobaru and M. Duangpanya, *A peridynamic formulation for transient heat conduction in bodies with evolving discontinuities*, J. Comput. Phys., 231 (2012), 2764-2785.

[9] N. Burch and R.B. Lehoucq, *Classical, nonlocal, and fractional diffusion equations on bounded domains*, Int. J. Multiscale Comput. Eng., 9 (2011), 661-674.

[10] X. Chen and M. Gunzburger, *Continuous and discontinuous finite element methods for a peridynamics model of mechanics*, Comput. Method Appl. Mech. Eng., 200 (2011), 1237-1250.

[11] W. C. Chew and W. H. Weedon, *A 3D perfectly matched medium from modified Maxwell equations with stretched coordinates*, Microw. Opt. Technol. Lett., 7:13 (1994), 599-604.

[12] P. N. Demmie and S. A. Silling, *An approach to modeling extreme loading of structures using peridynamics*, J. Mech. Mater. Struct., 2:10 (2007), 1921-1945.

[13] Q. Du, M. Gunzburger, R. Lehoucq and K. Zhou, *Analysis and approximation of nonlocal diffusion problems with volume constraints*, SIAM Rev., 54 (2012), 667-696.

[14] Q. Du, M. Gunzburger, R.B. Lehoucq and K. Zhou, *A nonlocal vector calculus, nonlocal volume-constrained problems, and nonlocal balance laws*, Math. Mod. Meth. Appl. Sci., 23 (2013), 493-540.

[15] Q. Du and K. Zhou, *Mathematical analysis for the peridynamic nonlocal continuum theory*, ESIAM: Math. Model. Numer. Anal., 45 (2011), 217-234.

[16] E. Emmrich and O. Weckner, *Analysis and numerical approximation of an integro-differential equation modelling non-local effects in linear elasticity*, Math. Mech. Solids, 12 (2007), 363-384.

[17] E. Emmrich and O. Weckner, *On the well-posedness of the linear peridynamic model and its convergence towards the Navier equation of linear elasticity*, Commun. Math. Sci., 5 (2007), 851-864.

[18] E. Emmrich and O. Weckner, *The peridynamic equation and its spatial discretisation*, Math. Model. Anal., 12:1 (2007), 17-27.

[19] B. Engquist and A. Majda, *Absorbing boundary conditions for the numerical simulation of waves*, Math. Comput., 31 (1977), 629-651.

[20] W. Gerstle, S. A. Silling, D. Read, V. Tewary, and R. Lehoucq, *Peridynamic simulation of electromigration*, Comput. Mater. Continua, 8:2 (2008), 75-92.

[21] D. Givoli, *Finite element analysis of heat problems in unbounded domains*, Numerical Methods in Thermal Problems 6.Part 2 (1989): 1094-1104.

[22] M. Gunzburger and R.B. Lehoucq, *A nonlocal vector calculus with application to nonlocal boundary value problems*, Multiscale Model. Simul., 8 (2010), 1581-1598.

[23] Y. D. Ha and F. Bobaru, *Studies of dynamic crack propagation and crack branching with peridynamics*, Int. J. Fract., 162:1-2 (2010), 229-244.

[24] H. Han and Z. Huang, *Exact and approximating boundary conditions for the parabolic problems on unbounded domains*, Comput. Math. Appl., 44 (2002), 655-666.

[25] H. Han and Z. Huang, *A class of artificial boundary conditions for heat equation in unbounded domains*, Comput. Math. Appl., 43 (2002), 889-900.

[26] H. Han and X. Wu, *Artificial Boundary Method*, Spring-Verlag and Tsinghua Unversity Press, Berlin Heidelberg and Beijing, 2013.

[27] S. Jiang, *Fast Evaluation of the Nonreflecting Boundary Conditions for the Schrödinger Equation*, Ph.D. thesis, Courant Institute of Mathematical Sciences, New York University, New York, 2001.

[28] S. Jiang and L. Greengard, *Fast Evaluation of Nonreflecting Boundary Conditions for the Schrödinger Equation in One Dimension*, Comput. Math. Appl., 47 (2004), no. 6-7, 955-966.

[29] S. Jiang and L. Greengard, *Efficient representation of nonreflecting boundary conditions for the time-dependent Schrödinger equation in two dimensions*, Comm. Pure Appl. Math., 61 (2008), 261-288.

[30] S.D. Jiang et al., *Fast evaluation of the Caputo fractional derivative and its applications to fractional diffusion equations*, preprint.

[31] J. Li, *A fast time stepping method for evaluating fractional integrals*, SIAM J. Sci. Comput., 31 (2010), 4696-4714.

[32] Y. Lin and C. Xu, *Finite difference/spectral approximations for the time-fractional diffusion equation*, J. Comput. Phys., 225 (2007), 1533-1552.

[33] R.W. Macek and S. Silling, *Peridynamics via finite element analysis*, Finite Elem. Anal. Des., 43 (2007), 1169-1178.

[34] T. Mengesha and Q. Du, *Analysis of a scalar peridynamic model with a sign changing kernel*, Disc. Cont. Dyn. Systems B, 18 (2013), 1415-1437.

[35] T. Mengesha and Q. Du, *Characterization of function spaces of vector fields via nonlocal derivatives and an application in peridynamics*, Nonlinear Anal. A, 140 (2016), 82-111.

[36] R. Metzler and J. Klafter, *The restaurant at the end of the random walk: Recent developments in the description of anomalous transport by fractional dynamics*, J. Phys. A, 37 (2004), R161.

[37] S. P. Neuman and D. M. Tartakovsky, *Perspective on theories of non-Fickian transport in heterogenous media*, Adv. Water Resources, 32 (2009), 670-680.

[38] K.B. Oldham and J. Spanier, *The Fractional Calculus*, Academic Press, New York, 1974.

[39] S. A. Silling and E. Askari, *A meshfree method based on the peridynamic model of solid mechanics*, Comput. Struct., 83:17-18 (2005), 1526-1535.

[40] S. Silling and R.B. Lehoucq, *Peridynamic theory of solid mechanics*, Adv. Appl. Mech., 44 (2010), 73-166.

[41] S. Silling, O. Weckner, E. Askari and F. Bobaru, *Crack nucleation in a peridynamic solid*, Int. J. Fracture, 162 (2010), 219-227.

[42] Z. Sun and X. Wu, *A fully discrete difference scheme for a diffusion-wave system*, Appl. Numer. Math., 56 (2006), 193-209.

[43] X. Tian and Q. Du, *Analysis and comparison of different approximations to nonlocal diffusion and linear peridynamic equations*, SIAM J. Numer. Anal., 51 (2013), 3458-3482.

[44] X. Tian and Q. Du, *Asymptotically compatible schemes and applications to robust discretization of nonlocal models*, SIAM J. Numer. Anal., 52 (2014), 1641-1665.

[45] R.A. Wildman and G.A. Gazonas, *A perfectly matched layer for peridynamics in two dimensions*, J. Mech. Mater. Struct., 7:8-9 (2012), 765-781.

[46] R.A. Wildman and G.A. Gazonas, *A perfectly matched layer for peridynamics in one dimension*, Technical report ARL-TR-5626, U.S. Army Research Laboratory, Aberdeen, MD, 2011.

[47] X. Wu and J. Zhang, *High order local absorbing boundary conditions for heat equation in unbounded domains*, J. Comput. Math., 29 (2011), 74-90.

[48] C. Zheng, *Approximation, stability and fast evaluation of exact artificial boundary condition for one-dimensional heat equation*, J. Comput. Math., 25 (2007), 730-745.

[49] K. Zhou and Q. Du, *Mathematical and Numerical Analysis of Linear Peridynamic Models with Nonlocal Boundary Conditions*, SIAM J. Numer. Anal., 48 (2010), 1759-1780.